Electronic Supplementary Material (ESI) for Journal of Materials Chemistry C.
This journal is © The Royal Society of Chemistry 2017

Electronic Supplementary Information for

"Morphological Regulation Improved Electrical Conductivity and Electromagnetic Interference Shielding in Poly(L-lactide)/Poly(ε-caprolactone)/Carbon Nanotubes Nanocomposites via Constructing Stereocomplex Crystallites in Poly(L-lactide) Phase"

Kai Zhang,[a] Hai-Ou Yu,[a] Yu-Dong Shi,[a] Yi-Fu Chen,[a]

Jian-Bing Zeng,[a] Jiang Guo,[b] Bin Wang,[b,c] Zhanhu Guo[b*] and Ming Wang[a*]

[a]Key Laboratory of Applied Chemistry of Chongqing Municipality, School of Chemistry and Chemical Engineering, Southwest University, Chongqing, 400715, China

[b]Integrated Composites Laboratory (ICL),
Department of Chemical and Biomolecular Engineering,
University of Tennessee, Knoxville, TN, 37996, USA

[c] Engineered Multifunctional Composites (EMC) Nanotechnology LLC,
Knoxville, TN 37934 USA

*Corresponding Author
E-mail address: mwang@swu.edu.cn (M. Wang),

nanomaterials2000@gmail.com or zguo10@utk.edu (Z. Guo).

1. Crystallization behavior of the (*x*PLLA+*y*PDLA)/PCL/*z*MWCNTs nanocomposites

In order to investigate the nucleating effect of SCs for PLLA HCs, the samples with PDLA was analyzed by the nonisothermal crystallization. Before crystallization, all samples were kept for 3 min at 190 °C (above the melting point of HCs but below that of SCs) at which only HCs were melted, and SCs were reserved. For the samples without PDLA, only the PCL crystallization peak was found, indicating the PLLA hardly crystallized at the cooling rate of 10 °C/min, as shown in Figure S1a. With the incorporation of MWCNTs, the crystallization temperature (T_c) shifts to higher temperature compared to that of the PLLA/PCL blends due to its heterogeneous nucleating effect on PCL chains.

For the samples with PDLA, the crystallization of PLLA happened during the cooling at a rate of 10 °C/min. The T_c of the HCs was 119 ^{o}C, as shown in Figure S1b, indicating the crystallization behavior of PLLA was greatly improved. The improvement of the PLLA HCs was ascribed to the nucleating effect of SCs on the formation of HCs. Furthermore, the addition of PDLA in PLLA phase showed almost no effect on the crystallization behavior of PCL phase.

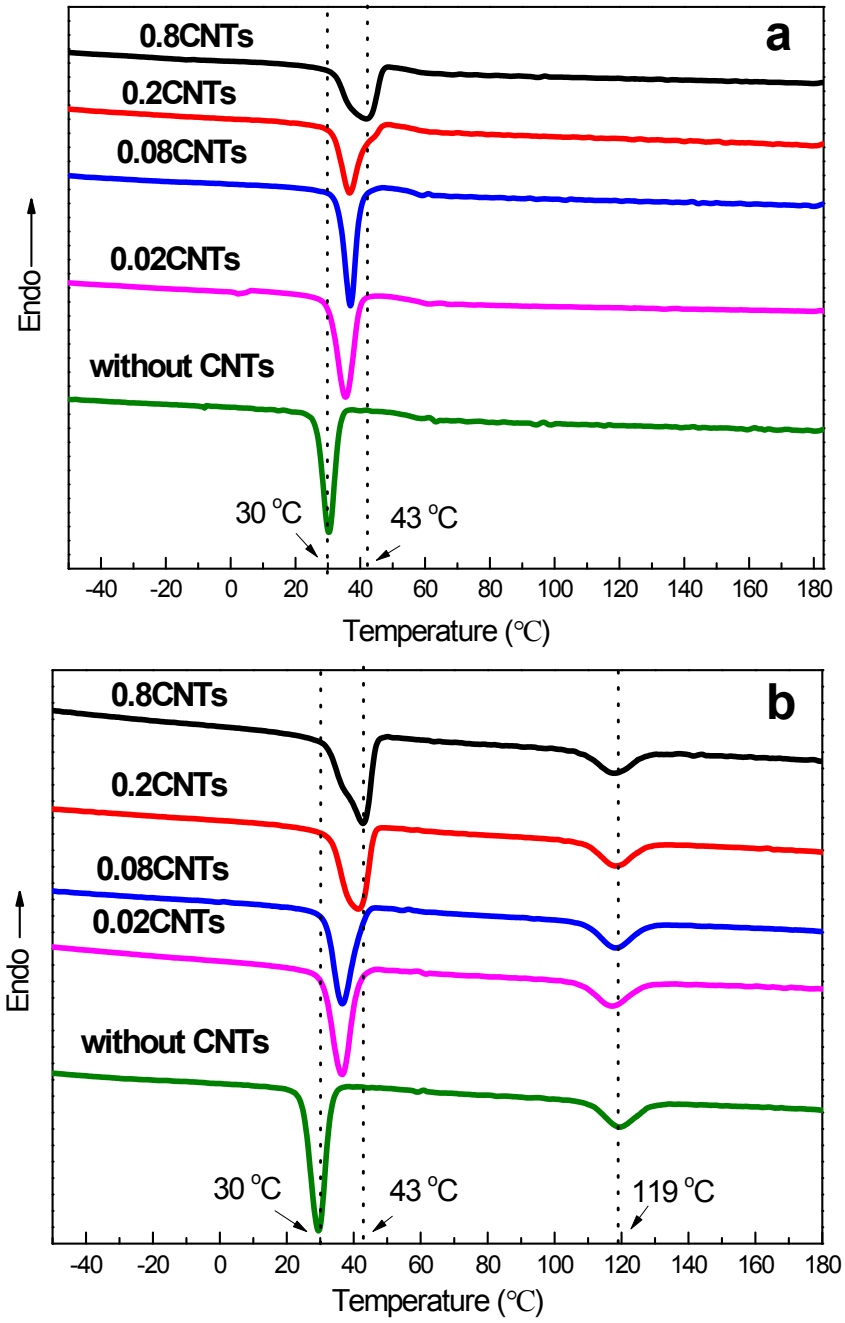

Fig. S1 Crystallization curves of the PLLA/PCL/*z*MWCNTs nanocomposites (a) and the (48PLLA+12PDLA)/PCL/*z*MWCNTs nanocomposites (b) collected upon cooling at a cooling rate of 10 °C/min.

2. Rheological behaviors of the PLLA/PDLA bends

In order to evaluate the increase viscosity by SCs, the rheological behaviors of the PLLA and PDLA bends with different ratio were measured on a rotational rheometer (TA AR200ex) with

two parallel plates. The dynamic frequency sweep mode was used with a strain of 0.1 % from 0.1 to 100 rad/s at 180 °C which is between the T_m of HCs and SCs.

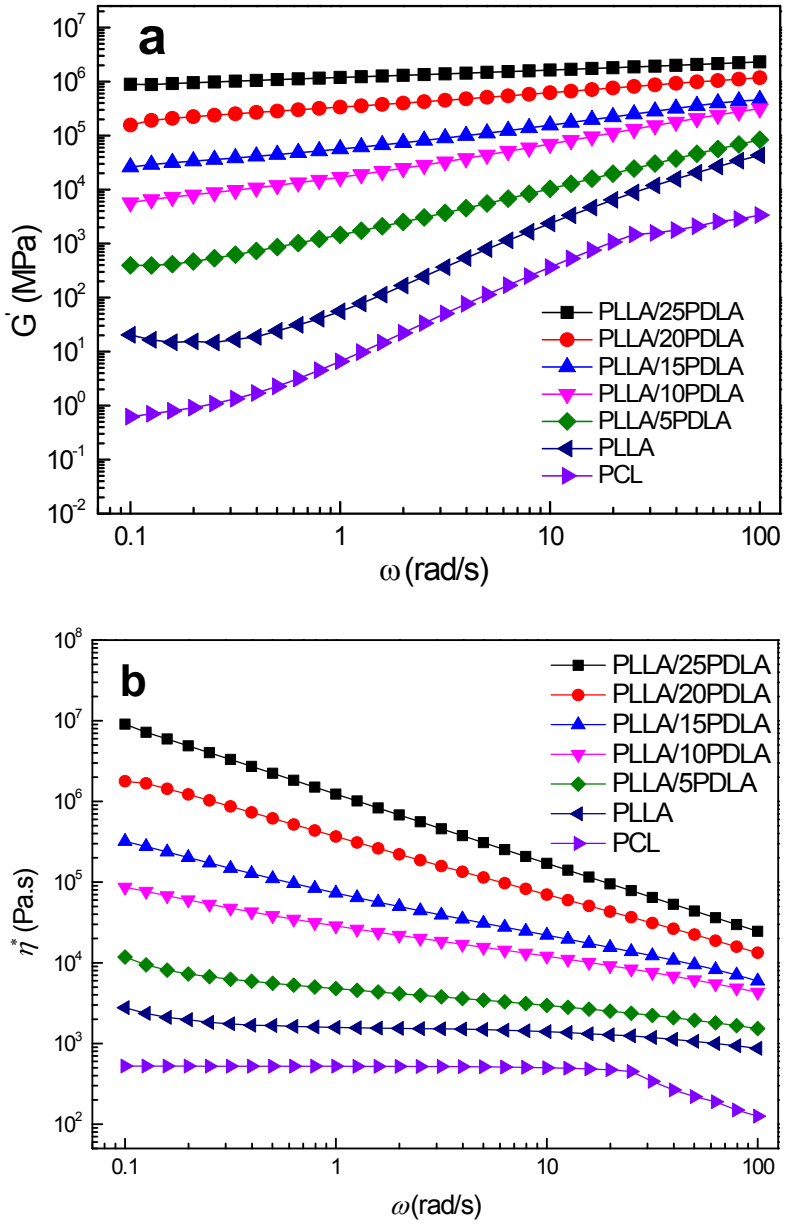

Fig. S2 Plots of the storage modulus (G') (a) and the complex viscosity (η^*) (b) vs. angular frequency (ω) of pure PCL and the PLLA/PDLA blends with different mixing ratios. The measurements were carried out with a strain of 0.1% at 180 °C.

Figure S2a shows the variation of storage modulus with frequency. The storage modulus of PLLA is obviously enhanced by adding 5 wt% PDLA. With further increasing PDLA

concentration up to 25 wt %, this enhancement becomes much pronounced, indicating that the SCs can significantly reinforces the melt elasticity of the PLLA matrix. The complex viscosity of PLLA also increases with the addition of PDLA, as shown in Figure S2b. According to the classical Paul-Barlow theory, the phase morphology of a dual-phase polymer blend is dependent on the composition and the melt-viscosity ratio between the two polymers. The composition at morphological inversion point can be predicted by the *equation S1*.

$$\frac{C_A}{C_B} = \frac{\eta_A}{\eta_B} \tag{S1}$$

where C_i and η_i represent the volume fraction and melt viscosity of component *i*, respectively. In general, the morphological transition from a sea-island structure to a cocontinuous can be achieved by changing the viscosity ratio and/or the components. The average shear rates our melt-processing in the internal mixer which is estimated by the Bousmina model [S1] is about 64.3 rad/s. The morphological inversion compositions of the PLLA/PCL blends with various PDLA concentrations are calculated from the *equation S1*and listed in Table S1.

Table S1. The calculated morphological inversion compositions for PLLA/PCL blends without and with various amounts of PDLA.

PDLA concentration (wt%)	0	5	10	15	20	25
Morphological inversion composition (wt/wt)	84/16	90/10	96/4	97/3	98/2	99/1

However, the final morphologies of the PLLA/PCL blends without or with PDLA are inconsistent with the theoretical prediction. For examples, the morphological inversion of

PLLA/PCL blends without PDLA happens at PLLA/PCL 50/50 blends. This large derivation from a theoretical prediction suggests that, besides the melt-viscosity ratio, the interfacial tension and the melt elasticity [S2-S5] which are not taken into account in the Paul−Barlow theory might also play an important role in the formation of network like PCL structure. A similar phenomenon was also reported in PLLA/PCL blends and was ascribed to higher elasticity for PLLA than PCL [S6]. Furthermore, the SCs embedded in the melt of PLLA can sharply enhance viscosity and elasticity of PLLA melt due to the filler effect and crosslinking effect of the SCs network. Thus, the morphologies can probably be regulated by constructing the SCs in PLLA phase.

3. Electrical conductivity of PCL/MWCNTs nanocomposites

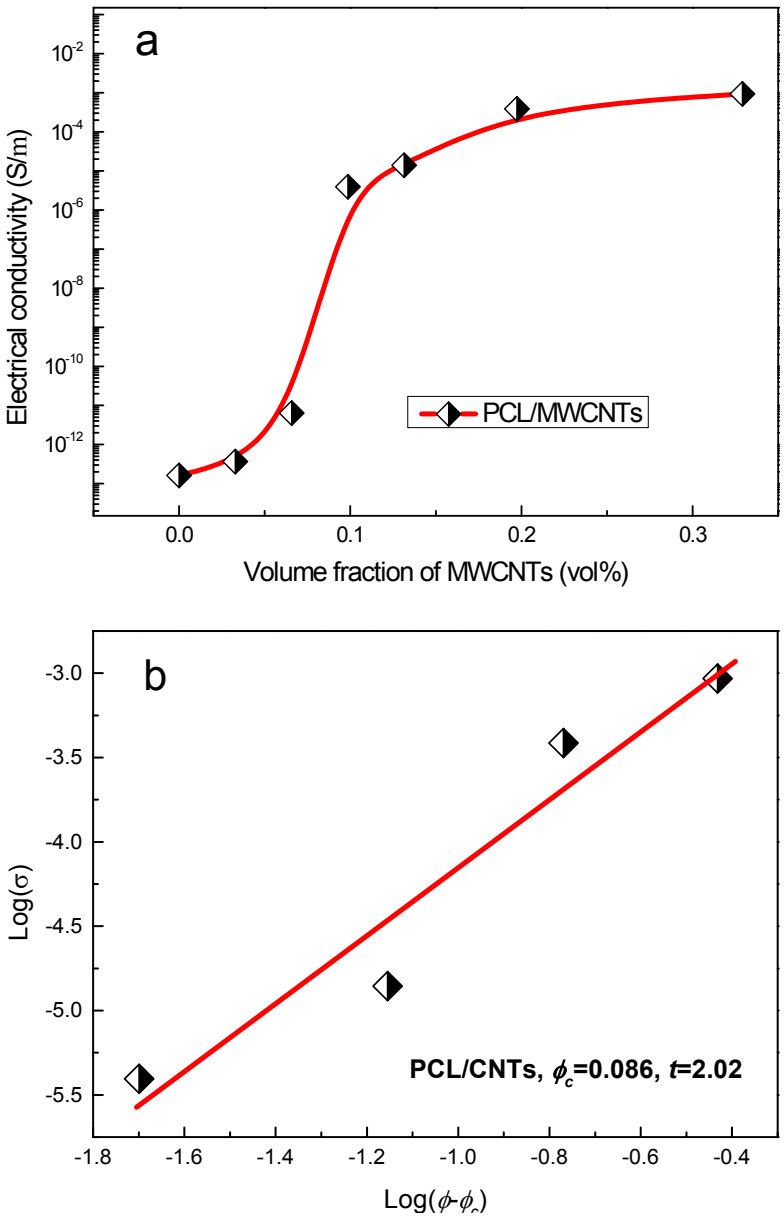

Fig. S3 Electrical conductivity of the PCL/MWCNTs nanocomposites as a function of MWCNTs loadings (a), the log−log plot of electrical conductivity versus ϕ-ϕ_c for the PCL/MWCNTs nanocomposites (b).

According to *equation 2*, the percolation threshold ϕ_c of the PCL/MWCNTs nanocomposites is estimated to be 0.086 vol%, whereas the critical exponent t was 2.02.

4. SEM images of the composites with 0.2 wt% MWCNTs

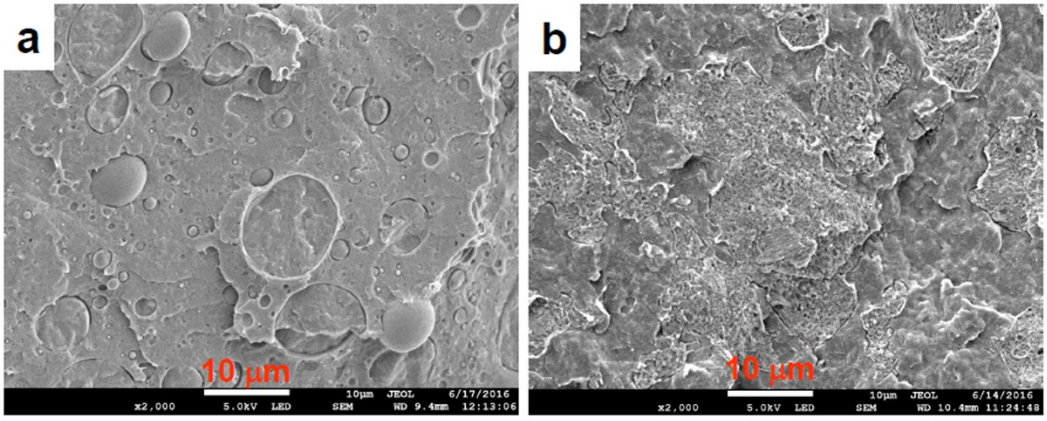

Fig. S4 SEM images of the PLLA /PCL/*z*MWCNTs nanocomposites (a) and the (48PLLA+12PDLA)/PCL/*z*MWCNTs nanocomposites (b) with 0.2 wt% MWCNTs.

5. Thermodynamic and kinetic analysis for the localization of MWCNTs in the PLLA/PCL/MWCNTs composites

The localization of MWCNTs in the PLLA/PCL/MWCNTs nanocomposites were first estimated by calculation of the wetting coefficient (ω)[S7-S11]

$$\omega = \frac{\gamma_{MWCNT-b} - \gamma_{MWCNT-a}}{\gamma_{ab}} \tag{3}$$

where $\gamma_{MWCNT-a}$ and $\gamma_{MWCNT-b}$ are the interfacial energy respectively between MWNTs and component *a*, between MWNTs and component *b*, respectively, and γ_{ab} is the interfacial tension between the two components. If the wetting coefficient is higher than 1, the filler will preferentially be located in component *a*; if the wetting coefficient is lower than -1, the filler will preferentially be located in component *b*, and if the wetting coefficient is between -1 and 1, the filler will be located at the interface between the two components.

In this work, the melt mixing temperature is 180 °C. Thus, it is necessary to extrapolate the surface energies towards this temperature. In order to obtain the high temperature data, the polymer polarity is assumed to be independent on the temperature. The surface parameter values (180 °C) of PLLA and PCL (see Table S2) were extrapolated from the experimental 25 °C values using the temperature coefficients of 0.06[S12] and 0.058 [S13] $mN \cdot m^{-1} \cdot K^{-1}$, respectively. Table S3 shows the interfacial energies of the sample pair. The wetting coefficient of PLLA/PCL/MWCNTs composites at both 25 °C and 180 °C are shown in Table S4. All the wetting coefficient values are lower than -1, which means that the MWCNTs are preferably to locate in PCL phase.

Table S2. Surface tensions of pure PLLA and pure PCL at 25 °C and 180 °C which extrapolated from values at 25 °C. The surface tensions of MWCNTs were obtained from the reference[S14].

Samples	Total (γ),(mN/m)	dispersive part (γ^d), (mN/m)	polar part (γ^p), (mN/m)
MWCNTs	27.8	17.6	10.2
PLLA (25 °C)	43.2	39.2	3.9
PLLA (180 °C)	33.9	30.8	3.1
PCL(25 °C)	38.4	36.5	1.9
PCL(180 °C)	29.4	26.9	1.5

Table S3. The calculated values of interfacial energies for various sample pairs.

Sample pair	Interfacial energies(mN/m) Calculation methods	
	harmonic	geometric
PLLA (25 °C)/MWCNTs	11.1	5.9
PLLA (180 °C) /MWCNTs	7.4	3.9
PCL (25 °C)/MWCNTs	12.3	6.7
PCL (180 °C) /MWCNTs	9.4	5.9
PCL (180 °C)/ PLLA (180 °C)	1.8	1.4
PCL(25 °C) /PLLA (25 °C)	0.8	0.4

Table S4. Wetting coefficient evaluated according harmonic mean equation, geometric mean equation.

Materials	Wetting coefficient Calculation methods	
	harmonic	geometric
PLLA (25 °C)/PCL (25 °C)/MWCNTs	-1.5	-2.0
PLLA (180 °C)/PCL (180 °C)/MWCNTs	-1.1	-1.4

However, it is well known that the location of MWCNTs is also dependent on the melts viscosity of polymer pairs, which is the kinetic factor.[S15] Fig. S2 shows the different viscosity of PCL and PLLA melts at 180 °C. It is obvious that the melt viscosity of PCL is much lower than that of PLLA within the experiment range. The shear rate applied in the melt-mixing process was 80 rpm, which was estimated to be 8.38 rad/s according to the conversion law: 1 rad/s = 9.55 rpm. The viscosity ratio between PLLA and PCL melt is about 3.0 at 8.38 rad/s. It has been reported that the MWCNTs have a tendency to localize in the lower viscosity PCL phase [S8]. The results indicate that PCL chains are more readily to diffuse around and into the MWCNTs aggregates compared with that of the PLLA chains during melt mixing and, the MWCNTs are incorporated inside the low viscous PCL phase preferentially and finally trapped inside it. Therefore, the

MWCNTs actually located in PCL phase by the kinetic aspects in our case, which is consistent with the SEM results.

From the thermodynamic analysis, the MWCNTs prefer to locate in the PLLA phase. However, it can't be achieved at our mixing condition because of the kinetic factor which leads to the MWCNTs being trapped in the PCL phase.

References

S1 M. Bousmina, A. Ait-Kadi and J. B. Faisant, *J. Rheol.* 1999, **43**, 415-433.

S2 R. C. Willemse, A. P. de Boer, J. van Dam and A. D. Gotsis, *Polymer* 1999, **40**, 827-834.

S3 A. Nuzzo, S. Coiai, S. C. Carroccio, N. T. Dintcheva, C. Gambarotti and G. Filippone, *Macromol. Mater. Eng.* 2014, **299**, 31-40.

S4 Z. Xu, Y. Zhang, Z. Wang, N. Sun and H. Li, *ACS Appl. Mater. Interface* 2011, **3**, 4858-4864.

S5 Z. Liu, Y. Luo, H. Bai, Q. Zhang and Q. Fu, *ACS Sustainble Chem. Eng.* 2016, **4**, 1111-1120.

S6 D. F. Wu, Y. S. Zhang, M. Zhang and W. D. Zhou, *Eur. Polym. J.* 2008, **44**, 2171-2183.

S7 M. Sumita, K. Sakata, S. Asai, K. Miyasaka and H. Nakagawa, *Polym. Bull.,* 1991, **25**, 265.

S8 D. Wu, D. Lin, J. Zhang, W. Zhou, M. Zhang, Y. Zhang, D. Wang and B. Lin, *Macromol. Chem. Phys.,* 2011, **212**, 613-626

S9 A.-C. Baudouin, J. Devaux and C. Bailly, *Polymer*, 2010, **51**, 1341-1354

S10 Y. Lan, H. Liu, X. Cao, S. Zhao, K. Dai, X. Yan, G. Zheng, C. Liu, C. Shen and Z. Guo, *Polymer*, 2016, **97**, 11-19

S11 T. Gong, M.-Q. Liu, H. Liu, S.-P.Peng, T. Li, R.-Y. Bao, W. Yang, B.-H. Xie, M.-B. Yang and Z. Guo, *Polymer*, 2017, **110**, 1-11.

S12 A. Katada, Y. F. Buys, Y. Tominaga, S. Asai, and M. Sumita, *Colloid Polym. Sci.*, 2005, **284**, 134-141.

S13 D. Cava, R. Gavara, J. M. Lagaron, and A. Voelkel, *J. Chromatogr. A*, 2007, **1148**, 86-91.

S14 A. H. Barber, S. R. Cohen and H. D. Wagner, *Phys. Rev. lett.*, 2004, **92**, 186103.

S15 Y.-Y. Shi, J.-H. Yang, T. Huang, N. Zhang, C. Chen and Y. Wang, *Compos. Part B Eng.*, 2013, **55**, 463-469.